Polymers **2014**, *6*, 1877-1896; doi:10.3390/polym6071877

OPEN ACCESS

polymers

ISSN 2073-4360

www.mdpi.com/journal/polymers

Article

Stimuli-Responsive Polyelectrolyte Brushes As a Matrix for the Attachment of Gold Nanoparticles: The Effect of Brush Thickness on Particle Distribution

Stephanie Christau, Stefan Thurandt, Zuleyha Yenice and Regine von Klitzing *

Stranski-Laboratorium für Physikalische Chemie, Technische Universität Berlin, Strasse des 17, Juni 124, 10623 Berlin, Germany; E-Mails: stephanie.christau@campus.tu-berlin.de (S.C.); stefan.thurandt@gmx.de (S.T.); yenice@mailbox.tu-berlin.de (Z.Y.)

* Author to whom correspondence should be addressed; E-Mail: klitzing@mailbox.tu-berlin.de; Tel.: +49-(0)30-314-23476.

Received: 16 April 2014; in revised form: 23 June 2014 / Accepted: 24 June 2014 / Published: 27 June 2014

Abstract: The effect of brush thickness on the loading of gold nanoparticles (AuNPs) within stimuli-responsive poly-(*N,N*-(dimethylamino ethyl) methacrylate) (PDMAEMA) polyelectrolyte brushes is reported. Atom transfer radical polymerization (ATRP) was used to grow polymer brushes via a "grafting from" approach. The brush thickness was tuned by varying the polymerization time. Using a new type of sealed reactor, thick brushes were synthesized. A systematic study was performed by varying a single parameter (brush thickness), while keeping all other parameters constant. AuNPs of 13 nm in diameter were attached by incubation. X-ray reflectivity, electron scanning microscopy and ellipsometry were used to study the particle loading, particle distribution and interpenetration of the particles within the brush matrix. A model for the structure of the brush/particle hybrids was derived. The particle number densities of attached AuNPs depend on the brush thickness, as do the optical properties of the hybrids. An increasing particle number density was found for increasing brush thickness, due to an increased surface roughness.

Keywords: polymer brushes; gold nanoparticles; nanocomposite; atom transfer radical polymerization (ATRP); surface plasmon resonance; brush thickness

---

1. Introduction

Brushes that are tethered to a surface have attracted much interest in the last few years. Because they are chemically end-grafted to the substrate, they provide a higher stability than physically adsorbed films. Neutral polymer brushes and polyelectrolyte brushes are widely used for the modification of surfaces, due to their advantageous specific properties, such as mechanical and chemical stability, their adsorption behavior [1] and permeability [2] and the possibility to tune their structure by varying external stimuli. For instance, the structure of a weak polyelectrolyte brush depends on pH [3–8], temperature [9–11], salt [12–15] and solvent [16–18]. More precisely, the swelling/shrinking of the studied poly-(*N,N*-(dimethylamino ethyl) methacrylate) (PDMAEMA) brushes can be manipulated by adjusting the pH of the surrounding environment to values below and above the pK_A. PDMAEMA brushes are temperature-sensitive; they will be swollen below their lower critical solution temperature (LCST), and collapsed above the LCST (∼50–60 °C). Furthermore, it could be shown that the swelling/shrinking of PDMAEMA brushes can be manipulated by applying voltage. Positive voltages (positive electrode connected to the brush) were shown to cause swelling; negative voltages caused deswelling [19].

Polymer brushes cover a wide range of applications. Due to their responsive nature, they are an important tool for the development of smart surfaces and for sensor and actuator applications in nanotechnology [20–22]. Further, they come into play in biological applications [23–27] and for biomedical applications as drug delivery systems [2,28–33]. Brushes can be used as matrices for the immobilization of nanoparticles, resulting in nanocomposite materials with interesting features, such as tunable optical, magnetical or mechanical behavior. In the present study, polyelectrolyte brushes are used as a matrix for the immobilization of gold nanoparticles (AuNPs), which induce optical properties, due to their surface plasmon resonance (SPR) [34]. This can be exploited to construct a nanosensor, where the swelling/shrinking of responsive brushes can be monitored by detecting the surface plasmon resonance of the particles [20,22]. The brush/particle hybrids combine the specific properties of both materials. It is important to get a better understanding of particle self-assembly in the brush matrix to be able to tune the properties of the entire system.

It has been theoretically predicted that the interpenetration of particles strongly depends on particle size, brush grafting density and chain length (brush thickness) [35,36]. The interplay between those parameters will determine the structure of the formed brush/particle hybrid. Shorter brushes will induce 2D ordering of the particles. If the brushes are long enough, 3D ordering of particles should be observed, *i.e.*, the particles should interpenetrate into the brush system. Bhat *et al.* [34] studied the assembly of AuNPs in two and three dimensions by generating concentration gradients of a self-assembled monolayer as a 2D template and molecular weight gradients of poly(acryl amide) as the 3D template. Using scanning force microscopy and UV-Vis spectroscopy, they found an increased particle uptake with increasing polymer molecular weight [34]. Using two different brush heights, 5.5 and 10 nm, they found that small particles (3.5 nm) can only form 3D assemblies with the thicker brush. Larger particles (16 nm) did not interpenetrate into brushes of 5.5 and 13 nm thickness at all. However, the reported brushes are fairly thin with a dry thickness in the range of the particle size. In the present paper, the brush thickness is varied from a dry thickness in the range of the particle size to a dry thickness

approximately 10 times higher than the particle size. The mechanism of particle interpenetration and the complex internal interaction between brush, particles and solvent molecules is still unclear. Regarding this, the spatial distribution of the particles within the polymer brush is studied using X-ray reflectivity, a suitable tool to detect the inner structure of a material. Considering optical sensoring, a high particle density in the brush matrix is required to observe the particle-related surface plasmon resonance. 3D brush templates, which possess isolating properties and optical transparency, are ideal building blocks for the development of such optical devices.

In the present paper, the effect of brush thickness on particle loading will be reported. Variations in the spatial structure of the brush due to particle attachment will be discussed. Ellipsometry, X-ray reflectivity and scanning-electron microscopy will be combined to study the inner structure of the hybrid system. In order to achieve a systematic study, a new type of sealed reactor was used, which allows the preparation of samples where all parameters are fixed, except one (e.g., thickness). Brushes with a very high molecular weight (thickness) could be synthesized. This is also important for creating biosensors where a high brush thickness is required for a high signal-to-noise ratio to detect the analyte [37].

2. Experimental Section

2.1. Instruments

Ellipsometry: Ellipsometric measurements were performed with a polarizer-compensator sample analyzer (PCSA) ellipsometer (Optrel GbR, Sinzing, Germany), which works at a wavelength of 632.8 nm. The angle of incidence was set to 70° (a near Brewster angle of Si/air interface) for measurements under controlled humidity and ambient conditions and to 60° for measurements in water. A home-built humidity cell was used to perform measurements at different humidities, as introduced earlier [38]. For data manipulation, the software, Ellipsometry: simulation and data evaluation (Optrel, v. 3.1), was used. For the initiator-coated samples, a two-layer-model with air as the fronting (continuum, n = 1.000), silicon as the backing (continuum, $n = 3.885 - 0.180\,i$), silicon oxide as the first layer (n = 1.46) and the layer of the initiator as the second layer (n = 1.500) was assumed. For the brush samples, the model was expanded by a further layer, *i.e.*, a three-layer model was used for the calculation of thickness and the refractive index.

Atomic-force microscopy (AFM): Topographic imaging was carried out in air at room temperature with a Cypher AFM (Asylum Research, Santa Barbara, CA, USA) at scan rates between 1 and 2 Hz. For imaging, Al-coated silicon cantilevers (Olympus, Tokio, Japan) with a resonant frequency of 320 Hz, a tip radius of 10 nm, a length of 160 µm and a force constant of 42 N/m were used. The Asylum Research Software, a package of IgorPro (Wavemetrics, Inc., Portland, OR, USA), was used for data analysis. The surface roughness was calculated using the formula:

$$\sigma = \sqrt{\left(\frac{1}{N}\sum y_i^2\right)} \tag{1}$$

where σ is the root-mean-square roughness of the considered scan area, N is the number of pixels in this area and y_i is the z value of a specific pixel. To correct any tilting of the samples, all AFM images

were corrected using a line fit. The reported roughness was calculated out of three AFM measurements, which were taken at different positions of the wafer.

X-ray reflectivity (XRR): Measurements were carried out using a Bruker-AXS D8 Discover XRD diffraction system (Bruker AXS GmbH, Karlsruhe, Germany) long-fine focus KFLCu2K-tube at $\lambda_{\text{Cu-Ka}} = 0.1542$ nm. X-ray data were fitted with the IgorPro (Wavemetrics, Inc., Portland, OR, USA) package, Motofit [39]. The specular reflectivity is calculated using the Abeles [40] formulation as a function of the perpendicular momentum transfer Q_z:

$$Q_z = \frac{4\pi}{\lambda} sin\theta \tag{2}$$

The measured specular reflectivity (R) is the ratio of reflected intensity over incident intensity. A layer model was used for fitting the data with silicon as the backing (ρ_e = 0.71 Å^{-3}), air as the fronting (ρ_e = 0 Å^{-3}) and silicon oxide as the first layer (h = 1.5 nm, ρ_e = 0.71 Å^{-3}). For the polymer/brush particle hybrids, three layers were added.

Scanning Electron Microscopy (SEM): SEM measurements were carried out using a Zeiss DSM 982 GEMINI (LEO, Oberkochen, Germany). The SEM was operated at acceleration voltages of 5 kV for the thinnest brush sample and 8 kV for all the other samples in top view. For imaging the cross-sections, 20 kV were used for the thicker brush and 10 kV for the thinner brush.

Transmission Electron Microscopy (TEM): The samples were prepared using 5 µL of solution on a TEM copper grid with carbon support film (200 mesh, Science Services, Munich, Germany), which were pretreated using 10 s of a glow discharge. After drying, inserting into the sample holder (EM21010, JEOL GmbH, Eching, Germany) and transferring to a JEOL JEM 2100 (JEOL GmbH), TEM was carried out at an acceleration voltage of 200 kV. Images were recorded digitally using a bottom-mounted 4 k × 4 k CMOS camera system (TemCam-F416, TVIPS, Gauting, Germany) and processed with a digital imaging processing system (EM-Menu4.0, TVIPS).

2.2. Synthesis

For both the synthesis of the initiator-covered self-assembled monolayer and the synthesis of the brushes, a new reactor type was developed by the authors (Figure 1). The advantage of this reactor is that 16 samples can be placed inside at the same time, which can be removed independently while the polymerization is carried out. This is advantageous for tuning brush thickness by varying the polymerization time. If those 16 samples (previously coated with initiator) are placed in the reactor and ATRP is carried out, it is possible to remove them independently after different polymerization times. For example, the first sample can be removed after 1 h, the second sample after 2 h, *etc*. All other parameters that might affect the resulting brush (deoxygenation time, amount of dissolved CuCl in the solution, any sort of weighting errors, *etc.*) will be exactly the same for all 16 samples. The reaction is carried out under nitrogen, and nitrogen is pouring inside the reactor whenever a sample is removed to assure an oxygen-free atmosphere. The possibility of realizing different polymerization times by using only one reaction solution leads to directly comparable results.

Atom transfer radical polymerization (ATRP) was used to synthesize polyelectrolyte brushes via a "grafting from" approach. Control over the polymerization is obtained through dynamic equilibrium

between the active alkyl radicals and dormant alkyl halides [41]. ATRP was extensively reported, because it is easy to process and yields polymers with low polydispersity [42,43]. The ability to perform ATRP at room temperature [44] and in aqueous solution [43,45,46] was a huge progress in the history of ATRP. The activation rate of ATRP depends on many parameters, such as the ligand structure [47–49], the initiator structure [50,51], the solvent/temperature [52], Cu(II) [53,54] and the monomer [55]. The activating/deactivating transition metal species CuCl/$CuCl_2$ was used because of the preference for alkyl chlorides to be formed over alkyl bromides [56].

Figure 1. Schematic of the new reactor type developed for growing polymer brushes on flat substrates.

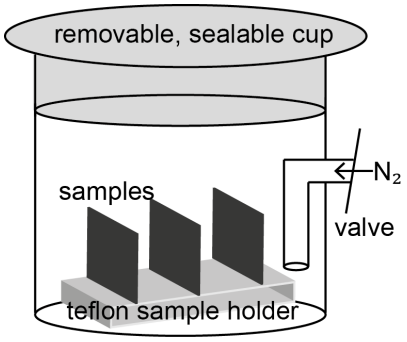

Chemicals: All chemicals used for synthesis were received from Aldrich and used without further purification.

Synthesis of the initiator, BTPAm: The synthesis of 2-bromo-2-methyl-*N*-(3-(triethoxysilyl)propyl) propanamide (BTPAm) was performed according to literature procedure [57]. A solution of toluene (25 mL) with α-bromoisobutyrate (BiBB) (0.825 mL, 6.6 mmol) was added dropwise to a cold solution of 2-aminopropyltriethoxysilane (APTES) (1.485 mL, 6.6 mmol) in toluene (20 mL) with triethylamine (TEA) (1.11 mL, 7.4 mmol) at 0 °C. The solution was magnetically stirred for 3 h at 0 °C and then for another 12 h at room temperature. For removal of the salts, the mixture was passed through filter paper and 3 times washed with toluene. The unreacted TEA was removed by evaporating the filtrate under reduced pressure. BTPAm was recovered as a yellowish oil, which could be characterized by ^{1}H-NMR: δ_H (400 MHz, $CDCl_3$/ TMS): 0.58 (2H, t, $SiCH_2$); 1.17 (9H, t, CH_3CH_2OSi); 1.58 (2H, m, CH_2); 1.96 (6H, s, CH_3C); 3.27 (2H, q, CH_2NH); 3.82 (6H, q, CH_3CH_2OSi); 6.85 (1H, s, NH). The product was stored under nitrogen, and another ^{1}H-NMR spectrum was recorded after 5 months to prove its stability.

Building a self-assembled monolayer (SAM) with the initiator BTPAm: As a first step, the substrates were etched using piranha solution (H_2SO_4/H_2O_2, 1:1 v/v). This procedure generates hydroxyl terminating groups and renders the surface hydrophilic and very reactive. The freshly cleaned substrates were placed into the reactor containing a 10 mM solution of BTPAm in anhydrous toluene. The whole setup was flushed with nitrogen for 15 min. The reactor was sealed and the reaction was carried out for 24 h at room temperature. After the reaction, the initiator-coated samples were rinsed with toluene, sonicated 5 min in toluene, cleaned with ethanol and dried under a stream of nitrogen.

ATRP of poly-(*N*,*N*-(dimethylamino ethyl) methacrylate (PDMAEMA): The synthesis was carried out following the literature [58], but with the difference of using the new reactor. Further, the literature recipe was modified by changing the CuCl/$CuCl_2$ ratio in order to slow down the reaction to achieve

more dense polymer brushes [59]. In a typical reaction protocol, 2,2'-bipyridyl (2.00 g, 12.80 mmol), 2-(dimethylamino ethyl) methacrylate (33.30 mL, 0.20 mol), ultrapure water (MilliQ, 19.2 m$\Omega\times$cm, 6.07 mL) and methanol (0.57 mL) are mixed in the reactor. Then, CuCl and $CuCl_2$ (variable amounts) were added quickly. At this point, the color of the solution changed from colorless to dark brown. After the mixture was deoxygenated for another 60 min by rigorous nitrogen bubbling under stirring (600 rpm), the initiator-coated substrates were put into the reactor under constant nitrogen flux. Then, the reactor was provided an airtight seal, and polymerization was conducted for a given polymerization time at room temperature. The polymerization was stopped after that time by exposing the reaction mixture to air. The substrates were sonicated in methanol and water, cleaned with acetone/ethanol and dried under a stream of nitrogen gas.

Synthesis of AuNPs: Spherical AuNPs of two different sizes were prepared following the literature [60] and provide citrate-coated particles. AuNP-13 were synthesized following a procedure, as first introduced by Enüstün and Turkevich [61]. One hundred milliliters of a $HAuCl_4$ solution (5×10^{-4} M) were heated (external heat $\approx$ 220 °C) under stirring at 500 rpm. At the time the $HAuCl_4$ solution started boiling, 5 mL of a 1 wt% sodium citrate solution were added quickly under continuous stirring at 500 rpm. After 3 min, the solution color changed to red. At this time, the external heat was reduced to 190 °C and the speed was reduced to 150 rpm. After 17 min, the heat was turned off, and the solution was stirred at 150 rpm overnight. The diameter of particles prepared by that method was found to be 13.24 $\pm$ 0.86 nm, as determined by TEM.

PDMAEMA/AuNP hybrids: AuNPs are adsorbed by incubation of the samples into the gold solution for at least 16 h to assure a high particle adsorption. In order to achieve the same conditions for the different samples, a special vessel was used where all samples can be incubated simultaneously with exactly the same time period and sample tilting (around 70°). After incubation, the samples were removed, sonicated in MilliQ water for 10 min to remove any loosely attached particles, cleaned with MilliQ twice and dried with nitrogen.

3. Results and Discussion

3.1. Results

3.1.1. Initiator Self-Assembled Monolayer (SAM)

For the BTPAm SAM, a thickness of 1.2 $\pm$ 0.1 nm was measured by ellipsometry. As previously reported in the literature, the theoretical value calculated from bond lengths of a stretched BTPAm molecule ($\sim$1.2 nm) is in the same range [57]. This validates the existence of a monolayer and not a multilayer. AFM images are generated at ambient conditions. The roughness was calculated from a (2×2) μm^2 area and displays a smooth surface (273 $\pm$ 33 pm).

3.1.2. PDMAEMA Brushes

Variation of the brush thickness (molecular weight): The brush thickness can be tuned by varying the polymerization time or ratio of activator/deactivator CuCl/$CuCl_2$ (see the Supporting Information). In

the present study, the brush thickness was adjusted by varying the polymerization time. This approach allows the preparation of samples within the same polymerization solution using the new reactor and will lead to directly comparable results and, therefore, a systematic study. In contrast to that, several polymerization solutions must be prepared to adjust the thickness by varying the CuCl/$CuCl_2$ amount. Different polymerization solutions will induce several varying parameters in addition to brush thickness. It should be pointed out that the samples obtained from Cu(I)/Cu(II) 14:1 have been used for the attachment of the particles in the present study. The roughness of PDMAEMA brushes calculated using AFM images of (4 × 4) μm^2 is increasing with the brush thickness (Figure 2).

Figure 2. Dependence of AFM surface roughness recorded at ambient conditions on ambient brush thickness (as measured by ellipsometry).

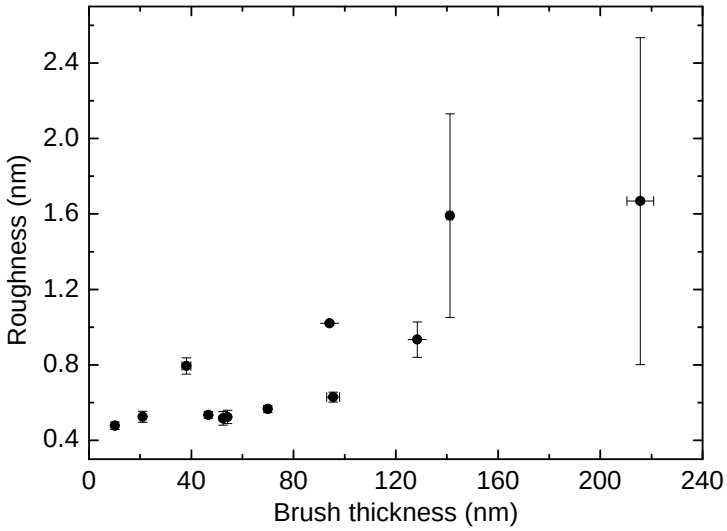

Swelling in humid air and water: The brush will be swollen during particle attachment (AuNPs are dissolved in water, a good solvent for PDMAEMA). Therefore, it is of interest to study the swelling behavior of the polymer before particle attachment. Swelling experiments of PDMAEMA brushes were carried out using ellipsometry for different relative humidities (<2%, 20%–30%, 50%–60%, 70%–80%, >90%) and in MilliQ water to study the effect of the brush thickness on the uptake of water. The water content in a swollen brush (in %) can be calculated using:

$$\text{Water content} = \frac{h_{sw} - h_{dry}}{h_{sw}} \times 100\% \quad (3)$$

where h_{sw} is the swollen thickness at the respective humidity (or in water) and h_{dry} is the dry thickness measured at <5% relative humidity (R.H.). The data show that there is no systematic change of the water uptake for the different brush heights, neither for swelling in humid air (Figure 3), nor for swelling in water (Figure 4). Due to water uptake in the brush, the refractive index (which was also fitted) is decreasing for increasing humidity (see the Supporting Information).

Figure 3. Water uptake in dependence of the relative humidity for various poly-(*N*,*N*-(dimethylamino ethyl) methacrylate) (PDMAEMA) brush thicknesses.

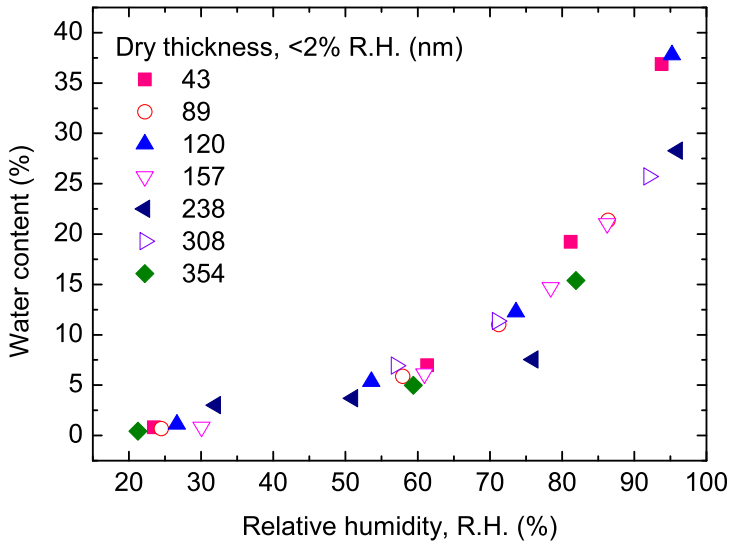

Figure 4. Water uptake of PDMAEMA brushes swollen in MilliQ water in dependence of brush thickness.

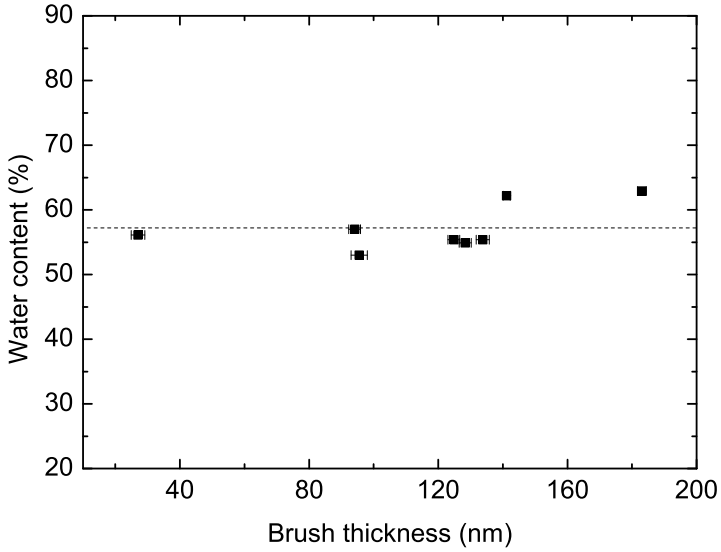

3.1.3. Brush/AuNP-13 Hybrids

Scanning electron microscopy (SEM): SEM was used to display the distribution and loading of attached nanoparticles on the polymer brushes (Figure 5). A high particle uptake was achieved for all brush thicknesses. SEM images of the cross-sections were collected from PDMAEMA/AuNP-13 with high thickness (200 nm, Figure 6b) and lower thickness (60 nm; Figure 6a). Both images show clearly that there is a dense layer of particles adsorbed at the polymer/air interface. Since the position of the

interface cannot be located from the images due to measurement conditions (80° sample tilting), SEM does not reveal whether the dense layer is formed as a mono- or a multi-layer.

Figure 5. SEM images of PDMAEMA/AuNP-13 hybrids with different thickness. Images were recorded in top view.

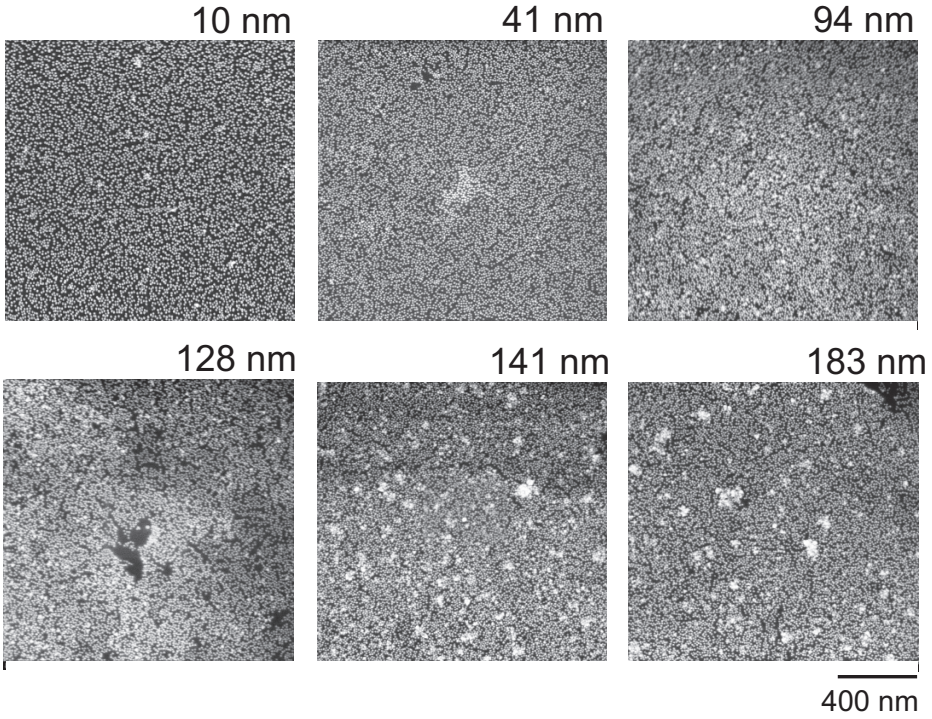

Figure 6. SEM cross-section images of the PDMAEMA/AuNP-13 hybrid with a (**a**) 60 nm and (**b**) a 200 nm thickness measured at 80° sample tilting.

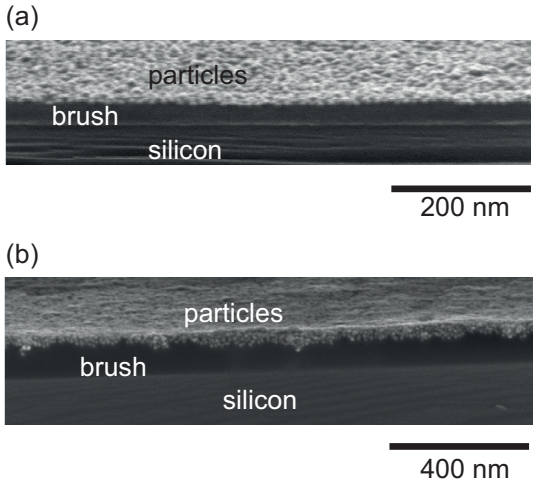

X-ray reflectivity (XRR): Since the electron densities of a metal (Au) and a polymer (PDMAEMA) are extremely different, XRR can be used to elaborate if the particles form a mono- or a multi-layer on top of the brushes. A three-layer model was used to fit the reflectivity data with Layer 1 assigned as the layer closest to the substrate. Experimental data and best fits are shown in Figure 7, and the results are summarized in Table 1. The thickness of Layers 2 and 3 together is in the range of the particle size

(∼12 nm), which validates the existence of a particle monolayer. For Layer 2, high electron densities were found, increasing as a function of brush thickness, whereas the electron densities of Layer 3 are independent of thickness and very low.

Figure 7. Experimental X-ray reflectivity (XRR) data (symbols) measured at ambient conditions and fits (line) for different brush heights (top to bottom: 10 nm, 41 nm, 94 nm and 128 nm). The data were fitted using a three-layer model.

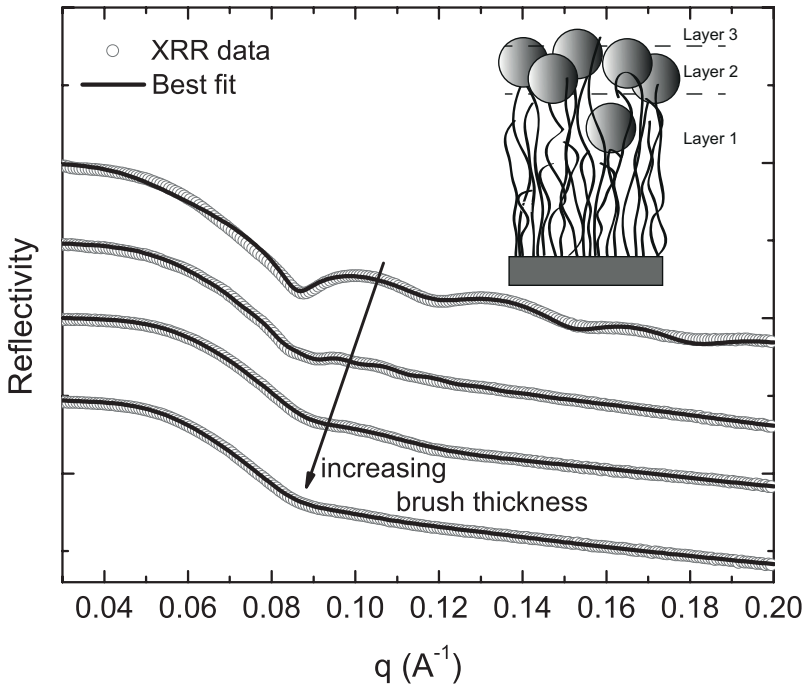

Table 1. Data for brushes and brush/particle hybrids (AuNP-13) with varying brush thickness obtained by X-ray reflectivity (XRR) measured at ambient conditions.

XRR Layer 1		**XRR Layer 2**		**XRR Layer 3**	
h_1 **(nm)**	$\rho_{e,1}$ **(Å^{-3})**	h_2 **(nm)**	$\rho_{e,2}$ **(Å^{-3})**	h_3 **(nm)**	$\rho_{e,3}$ **(Å^{-3})**
9	0.79	9	1.56	4	0.25
47	0.66	9	1.86	3	0.21
109	0.62	9	2.11	3	0.23
156	0.56	7	2.28	4	0.41

The total thickness increases after the attachment of AuNPs. This was also proven by scratching AFM (Table 2). Interestingly, the thickness of Layer 1 is higher than the total thickness of the brush before particle attachment (except for the thinnest brush). The swelling of Layer 1 can be calculated using:

$$\text{Swelling} = \frac{h_1 - h_{\text{PDM}}}{h_1} \times 100\% \tag{4}$$

where h_1 is the thickness of Layer 1 of the PDMAEMA/AuNP-13 hybrid and h_{PDM} is the thickness of the PDMAEMA brush before particle attachment. As shown in Figure 8, the swelling of Layer 1

increases with increasing hybrid thickness. The electron density found for Layer 1 is higher than the electron density for a pure PDMAEMA brush without particles, as determined by XRR to be ρ_e = 0.37 Å^{-3} (for data, see the Supporting Information). Additionally, the electron density is slightly decreasing with brush thickness. The mutual effect of swelling and electron density is shown in Figure 8 as a function of the hybrid thickness. For the thinnest brush, where no increase in the thickness of Layer 1 was observed, the swelling was set to zero.

Table 2. Total thickness of PDMAEMA brushes before particle attachment measured by ellipsometry compared to the thickness of PDMAEMA/AuNP-13 hybrids determined by AFM and XRR.

PDMAEMA	PDMAEMA/AuNP-13	
h_{Elli} (nm)	h_{AFM} (nm)	h_{XRR} (nm)
10 ± 0.3	20 ± 1	22
41 ± 2	51 ±2	58
94 ± 2	124 ± 3	121
128 ± 2	164 ± 4	167

Figure 8. Swelling of Layer 1 (squares) and electron density of Layer 1 (circles) as a function of PDMAEMA/AuNP-13 hybrid thickness.

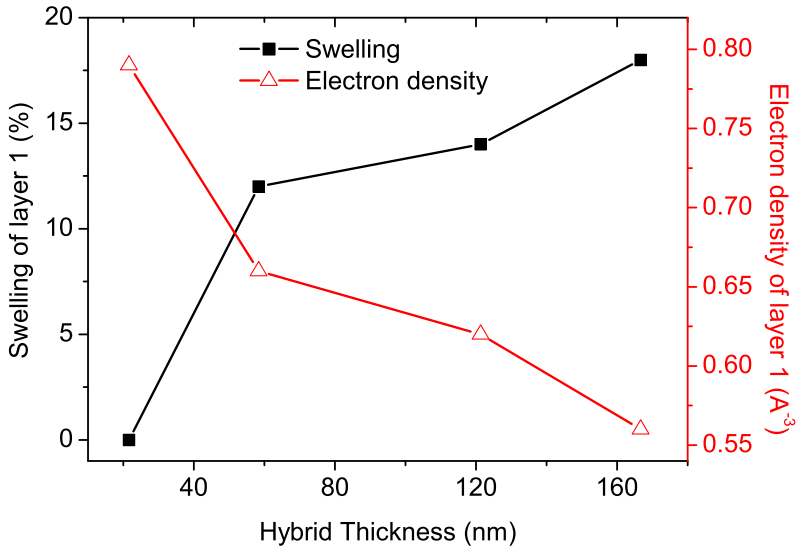

Taking into account the XRR electron densities, XRR layer thicknesses and SEM cross-section images, a model for the hybrid structure can be proposed (Figure 7, inset) with a monolayer of AuNPs attached on top of the brush and a very low amount of particles trapped inside Layer 1. Layer 3 is arising, because a certain roughness, due to the protruding of the particles, must be considered; the electron density of Layer 3 is therefore composed of polymer, particles and air, which is the reason for the lower value of the electron density.

Volume fractions: Knowing the electron densities ρ_e of components i and j of a hybrid system ij, the XRR volume fractions ϕ_i and ϕ_j, respectively, can be calculated using:

$$\rho_{e,\text{hybrid}} = \phi_i \rho_{e,i} + \phi_j \rho_{e,j}$$
$$= \phi_i \rho_{e,i} + (1 - \phi_i)\rho_{e,j} \quad (5)$$

where $\rho_{e,\text{hybrid}}$ is the electron density of the hybrid obtained by fitting the XRR data, exploiting $\phi_i + \phi_j = 1$. The XRR volume fractions of AuNPs in surface Layer 2 were calculated using electron densities of 4.5 Å^{-3} for gold (Motofit Database) and 0.37 Å^{-3} (measured by XRR, see the Supporting Information). They were found to be >30% and increase with increasing brush thickness up to 48%.

XRR particle numbers were calculated using:

$$\text{number of particles} = \frac{V_{\text{box}}}{V_{\text{AuNP}}} \quad (6)$$

where $V_{\text{AuNP}} = 4/3\pi r^3$ is the volume of one single AuNP with radius r = 6.5 nm. An imaginary box with volume V_{box} and a dimension of 1 µm length/width and 0.013 µm (= particle diameter) is designed (Figure 9). Assuming a perfectly flat monolayer attached on the brush surface, the box covers a (1 µm × 1 µm) area of the AuNP monolayer. Using Equation (6), the maximum number of particles within the designed box can be calculated (11,300 particles). This corresponds to a particle volume fraction of 100%. Using the calculated XRR volume fractions (30%–48%) it is possible to calculate the respective particle numbers attached within the box. Since the box height is equal to the particle size and the particles form a monolayer on top of the brushes, these values correspond to the particle number densities in terms of particles/µm^2. Number densities calculated from XRR volume fractions using the box model are assigned as XRR particle number densities.

Figure 9. Determination of XRR particle number densities by using a box model.

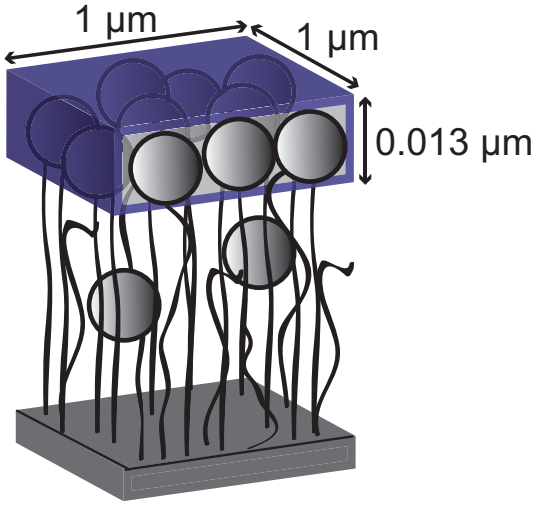

SEM particle number densities were determined from the respective SEM top view images (Figure 5) by image processing (ImageJ, Wayne Rasband, National Institutes of Health, Bethesda, MD, USA). For the thinner brushes (10 nm and 41 nm thickness), it is easier to distinguish between single attached particles, whereas for thicker brushes, a progressively nanoparticle crowding takes place until a maximum number of attached particles is reached (see also Figure 5). This maximum particle number

density was found to be ∼4000 particles/μm^2 and is reached for brush thicknesses >120 nm. Figure 10 shows a comparison between SEM and XRR particle number densities.

Figure 10. Particle number densities obtained by XRR (Layer 2) (squares) and SEM (circles) in dependence of PDMAEMA brush thickness.

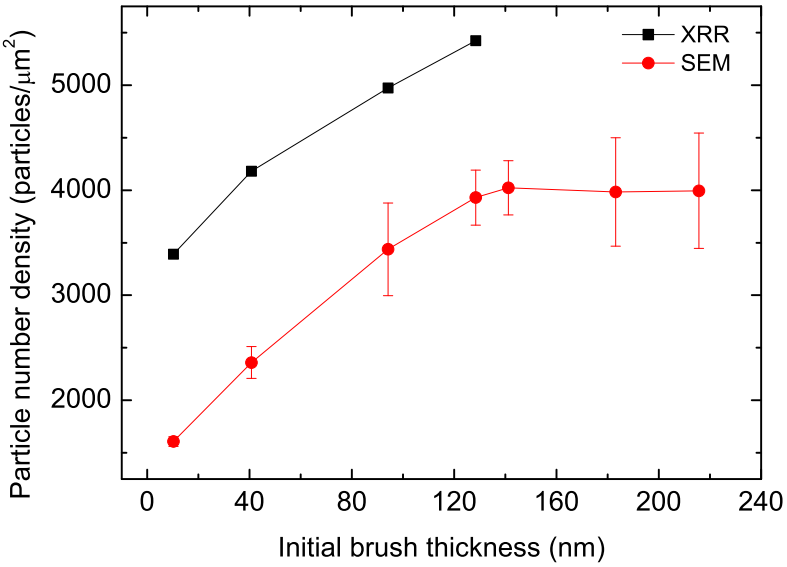

Both methods lead to the same qualitative behavior, although a higher particle number density was detected by XRR. There are two reasons for that. The described box model for the determination of the XRR particle number densities assumes a flat monolayer, neglecting the surface roughness. Due to this roughness, it may occur that one particle lies slightly beyond another particle. Thus, this particle might not be detected by SEM. Additionally, if the particles are close to each other, two particles might be detected as one particle by SEM image processing. Both will lead to a lower value for the SEM particle number densities compared to the respective value obtained by XRR, where all of the particles are detected in terms of the electron density. For XRR, only samples with initial brush thickness <140 nm were measured. Samples with higher thickness are too thick for the occurrence of Kiessig fringes, which allows no clear fitting results.

Ellipsometry: The optical properties of a material are described by the complex refractive index $\tilde{n} = n + ik$. The attached AuNPs induce an absorption term k into the hybrid system which can be measured by ellipsometry. Ellipsometric data of the PDMAEMA/AuNP-13 hybrids were collected at 21%–28% relative humidity to determine n and k; the thickness needed for fitting the data was known from scratching AFM measurements, which were carried out within the same humidity range. Figure 11 shows that n and k decrease as a function of brush thickness. The particle-related optical properties (absorption terms) are therefore decreasing as the brush thickness is increased.

Figure 11. The real part n and imaginary part k of the complex refractive index for PDMAEMA/AuNP-13 measured by ellipsometry.

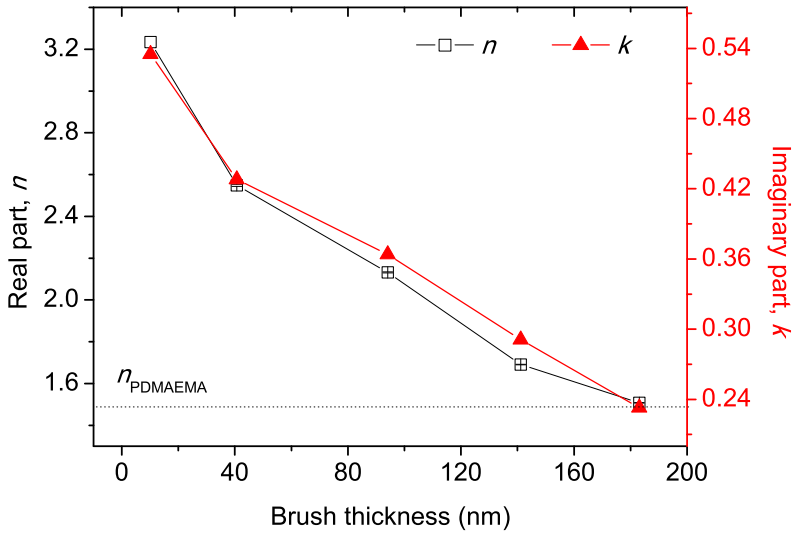

3.2. Discussion

The thickness of the PDMAEMA brushes increases linearly with polymerization time (see the Supporting Information) and, therefore, shows similar growth behavior as observed for other polymers, like polystyrene (PSS) [62] and (hydroxyethyl) methacrylate (HEMA) brushes [43]. The surface roughness of the tethered brushes was found to increase with increasing brush thickness (Figure 2). It could be shown that the water content within PDMAEMA brushes swollen in humid air or water is independent of the brush thickness (Figures 3 and 4). This is in agreement with recently published results from Rauch *et al.* [63], where the swelling ratios of PDMAEMA brushes in water were found to be independent of molecular weight.

Citrate-covered, negatively charged (zeta-potential around −40 mV) gold nanoparticles were attached by incubation. High particle uptake could be confirmed by SEM measurements. The pH of the gold solution (in water) is around 5.5–6. At this pH, PDMAEMA is positively charged (pK_A 7.5), and therefore, a strong attractive ionic interaction between particles and polymer is expected. For lower brush thickness, the particles are homogeneously distributed over the brush surface, each particle can be distinguished. However, for higher brush thickness, the particles are rather tightly packed, and it is getting difficult to obtain single particles attached to the brush. It could be shown that the surface particle number density increases with increasing brush thickness (Figure 10). This is attributed to increasing surface roughness, since more binding sites for adsorbing NPs become available, due to increasing surface area. SEM images of the cross-sections (Figure 6) show that the particles form a dense layer on top of the brushes.

Since the location of the polymer/air interface cannot be distinguished from these cross-section images, they yield no information about the number of detected layers and particle distribution. X-ray reflectivity was used to address this question. For the PDMAEMA/AuNP-13 hybrids, a three-layer model was used to fit the XRR data, where Layer 1 is the layer closest to the substrate. Layer 2, consisting of polymer and particles, shows the highest electron density due to attached AuNPs. The electron densities

of Layer 2 increase with increasing brush thickness and, therefore, confirm the results obtained from SEM, where the particle number density was found to increase with thickness. Layer 3 arises because a certain roughness must be considered; the particles are protruding out of the brush matrix. The electron density of Layer 3 is assumed to be a mixture of Au, PDMAEMA and mostly air, which explains the lower value of the electron density in Layer 3. Taking into account the obtained thicknesses, it is assumed that Layers 2 and 3 form a monolayer of particles attached at the brush surface. The electron densities of Layer 1 are slightly higher than the electron densities of a pure brush, revealing that a low amount of particles has interpenetrated into deeper regions of the brush.

Interestingly, the thickness of Layer 1 after particle attachment was found to be higher than the thickness of the pure brush before particle attachment. This effect gets more pronounced for increasing brush thickness. This could lead to the conclusion that more AuNPs have been attached within Layer 1 for increasing brush thickness. However, in that case, the electron density would have to increase with increasing brush thickness. However, this is not observed. In fact, the opposite behavior is found; the electron density decreases with increasing brush thickness. Decreasing electron density and simultaneously increasing thickness can be explained by an increasing water amount within the brush matrix. It is assumed that particle attachment will lead to the formation of cavities in the brush. Water will be trapped inside these cavities and will lead to an increased thickness. This swelling effect must be due to attached particles, because the swelling of pure PDMAEMA brushes was found to be independent of thickness. Further studies addressing "left-over" water in polymer brushes will be carried out.

A comparison of the SEM and XRR particle number densities shows the same trend: the particle number density increases with increasing brush thickness, and the slopes of the increase are the same for the SEM and XRR data. The particle number densities obtained from XRR are higher than the ones from SEM. The difference is due to the fact that a perfectly flat particle monolayer was assumed to determine XRR number densities, which is definitely an assumption, because the surface roughness of the brush was neglected.

In summary, the results lead to the conclusion that roughness is predominately affecting the particle attachment on the brush surface. Both roughness and particle uptake level off at a $\sim$120 nm brush thickness. Further particle absorption is hindered by electrostatic repulsion from already attached particles. Particles predominately stay at the brush surface; only a low amount of particles is attached within deeper regions of the brush.

The optical properties of the hybrid are a function of (1) brush thickness and (2) particle number density. For a fixed particle number density, the optical properties of the hybrid are progressively dominated by the polymer as the brush thickness is increasing. On the other hand, the particle-dominating optical properties of the hybrid will be enhanced for fixed brush thickness, while the particle number density is increasing. Figure 11 shows that n and k decrease as a function of brush thickness. The particle-related absorption term, decreasing with brush thickness, is therefore not dominated by the surface particle number density, which shows the opposite behavior (increases with thickness). The dominating factor for the average optical properties of the hybrid is the brush thickness.

4. Conclusions

The effect of the brush thickness on the loading of AuNPs on stimuli-responsive weak polyelectrolyte brushes, PDMAEMA, was investigated. Due to strong electrostatic interaction between positively charged polyelectrolyte brush and negatively charged AuNPs, a high particle loading was observed for each brush thickness. The particle number density increases with increasing brush thickness, due to increased surface roughness. A model for the structure of the hybrid was derived, where the particles form a monolayer attached on top of the brush, protruding out of the brush matrix. Further particle attachment is hindered due to a blocking effect by already adsorbed particles. A low amount of particles was found to be attached within deeper regions of the brush. Obviously, the brush is too dense to allow complete interpenetration of AuNP-13. Regarding better particle interpenetration, further studies will be carried out to optimize grafting density and particle size. Absorption coefficients decrease with thickness; the average optical properties of the hybrid are therefore dominated by the brush thickness. After attachment of AuNPs, the brushes are not able to shrink completely at ambient conditions. This effect was found to be dependent on the particle number density.

Acknowledgments

The authors gratefully thank Christoph Fahrenson (Zentraleinrichtung für Elektronenmikroskopie (ZELMI) , Technische Universität Berlin (TU)) for help with SEM measurements, Sarah T. Turner for TEM measurements and Kerstin Hansen (TU Berlin) for help with NMR measurements. TEM experiments were carried out at the electron microscope of the Joint Laboratory for Structural Research (JLSR) of Helmholtz-Zentrum Berlin für Materialien und Energie (HZB), Humboldt-Universität zu Berlin (HU) and Technische Universität Berlin (TU). Financial support was granted by the German Research Foundation (DFG) via the International Research Training Group (IRTG) 1524.

Author Contributions

All syntheses were carried out by Stephanie Christau. Ellipsometric humidity measurements were performed by Stefan Thurandt. Fitting of X-ray reflectivity data was done by Stephanie Christau. Zuleyha Yenice synthesized the gold nanoparticles. Stephanie Christau and Regine von Klitzing wrote the manuscript.

Conflicts of Interest

The authors declare no conflict of interest.

References

1. Andruzzi, L.; Senaratne, W.; Hexemer, A.; Sheets, E.D.; Ilic, B.; Kramer, E.J.; Baird, B.; Ober, C.K. Oligo(ethylene glycol) containing polymer brushes as bioselective surfaces. *Langmuir* **2005**, *21*, 2495–504.

2. Motornov, M.; Tam, T.K.; Pita, M.; Tokarev, I.; Katz, E.; Minko, S. Switchable selectivity for gating ion transport with mixed polyelectrolyte brushes: Approaching 'smart' drug delivery systems. *Nanotechnology* **2009**, *20*, doi:10.1088/0957-4484/20/43/434006.
3. An, S.W.; Thirtle, P.N.; Thomas, R.K.; Baines, F.L.; Billingham, N.C.; Armes, S.P.; Penfold, J. Structure of a diblock copolymer adsorbed at the hydrophobic solid/aqueous interface: Effects of charge density on a weak polyelectrolyte brush. *Macromolecules* **1999**, *32*, 2731–2738.
4. Houbenov, N.; Minko, S.; Stamm, M. Mixed polyelectrolyte brush from oppositely charged polymers for switching of surface charge and composition in aqueous environment. *Macromolecules* **2003**, *36*, 5897–5901.
5. Geoghegan, M.; Ruiz-Perez, L.; Dang, C.C.; Parnell, A.J.; Martin, S.J.; Howse, J.R.; Jones, R.A.L.; Golestanian, R.; Topham, P.D.; Crook, C.J.; *et al*. The pH-induced swelling and collapse of a polybase brush synthesized by atom transfer radical polymerization. *Soft Matter* **2006**, *2*, 1076–1080.
6. Plamper, F.A.; Schmalz, A.; Ballauff, M.; Mu, A.H.E. Tuning the thermoresponsiveness of weak polyelectrolytes by pH and light: Lower and upper critical-solution temperature of poly(N,N-dimethylaminoethyl methacrylate). *J. Am. Chem. Soc.* **2007**, *129*, 14538–14539.
7. Hinrichs, K.; Aulich, D.; Ionov, L.; Esser, N.; Eichhorn, K.J.; Motornov, M.; Stamm, M.; Minko, S. Chemical and structural changes in a pH-responsive mixed polyelectrolyte brush studied by infrared ellipsometry. *Langmuir* **2009**, *25*, 10987–10991.
8. Jia, H.; Wildes, A.; Titmuss, S. Structure of pH-responsive polymer brushes grown at the gold-water interface: Dependence on grafting density and temperature. *Macromolecules* **2012**, *45*, 305–312.
9. Balamurugan, S.; Mendez, S.; Balamurugan, S.S.; O'Brie, M.J.; Lopez, G.P. Thermal response of poly (N-isopropylacrylamide) brushes probed by surface plasmon resonance. *Langmuir* **2003**, *19*, 2545–2549.
10. Yim, H.; Kent, M.S.; Mendez, S.; Balamurugan, S.S.; Balamurugan, S.; Lopez, G.P.; Satija, S. Temperature-dependent conformational change of PNIPAM grafted chains at high surface density in water. *Macromolecules* **2004**, *37*, 1994–1997.
11. Liu, G.; Zhang, G. Collapse and swelling of thermally sensitive poly(N-isopropylacrylamide) brushes monitored with a quartz crystal microbalance. *J. Phys. Chem. B* **2005**, *109*, 743–747.
12. Biesalski, M.; Johannsmann, D.; Ruehe, J. Synthesis and swelling behavior of a weak polyacid brush. *J. Chem. Phys.* **2002**, *117*, 4988, doi:10.1063/1.1490924.
13. Currie, E.P.K.; Sieval, A.B.; Fleer, G.J.; Stuart, M.A.C. Polyacrylic acid brushes: Surface pressure and salt-induced swelling. *Langmuir* **2000**, *16*, 8324–8333.
14. Mouri, E.; Kaewsaiha, P.; Matsumoto, K.; Matsuoka, H.; Torikai, N. Effect of salt concentration on the nanostructure of weak polyacid brush in the amphiphilic polymer monolayer at the air/water interface. *Langmuir* **2004**, *20*, 10604–10611.
15. Zhang, H. Swelling of poly(methacrylic acid) brushes: Influence of monovalent salts in the environment. *Macromolecules* **2005**, *38*, 4855–4860.
16. Sanjuan, S.; Perrin, P.; Pantoustier, N.; Tran, Y. Synthesis and swelling behavior of pH-responsive polybase brushes. *Langmuir* **2007**, *23*, 5769–5778.

17. Biesalski, M.; Ruehe, J. Scaling laws for the swelling of neutral and charged polymer brushes in good solvents. *Macromolecules* **2002**, *35*, 499–507.
18. Ross, R.S.; Pincus, P. The polyelectrolyte brush: Poor solvent. *Macromolecules* **1992**, *25*, 2177–2183.
19. Weir, M.P.; Heriot, S.Y.; Martin, S.J.; Parnell, A.J.; Holt, S.A.; Webster, J.R.P.; Jones, R.A.L. Voltage-induced swelling and deswelling of weak polybase brushes. *Langmuir* **2011**, *27*, 11000–11007.
20. Gupta, S.; Agrawal, M.; Uhlmann, P.; Simon, F.; Oertel, U.; Stamm, M. Gold nanoparticles immobilized on stimuli responsive polymer brushes as nanosensors. *Macromolecules* **2008**, *41*, 8152–8158.
21. Mitsuishi, M.; Koishikawa, Y.; Tanaka, H.; Sato, E.; Mikayama, T.; Matsui, J.; Miyashita, T. Nanoscale actuation of thermoreversible polymer brushes coupled with localized surface plasmon resonance of gold nanoparticles. *Langmuir* **2007**, *23*, 7472–7474.
22. Tokareva, I.; Minko, S.; Fendler, J.H.; Hutter, E. Nanosensors based on responsive polymer brushes and gold nanoparticle enhanced transmission surface plasmon resonance spectroscopy. *J. Am. Chem. Soc.* **2004**, *126*, 15950–15951.
23. Cunliffe, D.; De, C.; Alarco, H.; Peters, V.; Smith, J.R.; Alexander, C. Poly(N-isopropylacrylamide) copolymers: Effect of phase transitions on protein and bacterial attachment. *Langmuir* **2003**, *19*, 2888–2899.
24. Hayashi, H.; Kono, K.; Takagishi, T. Temperature-controlled release property of phospholipid vesicles bearing a thermo-sensitive polymer. *Biochim. Biophys. Acta* **1996**, *1280*, 127–134.
25. Ista, L.K.; Pérez-luna, V.H.; López, G.P. Surface-grafted, environmentally sensitive polymers for biofilm release surface-grafted, environmentally sensitive polymers for biofilm release. *Appl. Environ. Microbiol.* **1999**, *65*, 1603–1609.
26. Langer, R.; Peppas, N.A. Advances in biomaterials, drug delivery, and bionanotechnology. *AIChE J.* **2003**, *49*, 2990–3006.
27. Stayton, P.S.; Shimoboji, T.; Long, C.; Chilkoti, A.; Chen, G.; Harris, J.M.; Hoffmann, A.S. Control of protein ligand recognition using a stimuli responsive polymer. *Nature* **1995**, *378*, 472–474.
28. Diamanti, S.; Arifuzzaman, S.; Genzer, J.; Vaia, R.A. Capture and release. *ACS Nano* **2009**, *3*, 807–818.
29. Bajpai, A.K.; Shukla, S.K.; Bhanu, S.; Kankane, S. Responsive polymers in controlled drug delivery. *Prog. Polym. Sci.* **2008**, *33*, 1088–1118.
30. Kost, J.; Langer, R. Responsive polymeric delivery systems. *Adv. Drug Deliv. Rev.* **2001**, *46*, 125–148.
31. Schmaljohann, D. Thermo- and pH-responsive polymers in drug delivery. *Adv. Drug Deliv. Rev.* **2006**, *58*, 1655–1670.
32. Pillai, O.; Panchagnula, R. Polymers in drug delivery. *Curr. Opin. Chem. Biol.* **2001**, *5*, 447–451.
33. De Las Heras Alarcon, C.; Pennadam, S.; Alexander, C. Stimuli responsive polymers for biomedical applications. *Chem. Soc. Rev.* **2005**, *34*, 276–285.
34. Bhat, R.R.; Genzer, J.; Chaney, B.N.; Sugg, H.W.; Liebmann-Vinson, A. Controlling the assembly of nanoparticles using surface grafted molecular and macromolecular gradients. *Nanotechnology* **2003**, *14*, 1145–1152.

35. Kim, J.; O'Shaughnessy, B. Morphology selection of nanoparticle dispersions by polymer media. *Phys. Rev. Lett.* **2002**, *89*, 238301.
36. Kim, J.U.; O'Shaughnessy, B. Nanoinclusions in dry polymer brushes. *Macromolecules* **2006**, *39*, 413–425.
37. Biesalski, M.; Ruehe, J. Swelling of a polyelectrolyte brush in humid air. *Langmuir* **2000**, *11*, 1943–1950.
38. Balzer, B.N.; Micciulla, S.; Dodoo, S.; Zerball, M.; Gallei, M.; Rehahn, M.; von Klitzing, R.; Hugel, T. Adhesion property profiles of supported thin polymer films. *ACS Appl. Mater. Interfaces* **2013**, *5*, 6300–6306.
39. Nelson, A. Co-refinement of multiple-contrast neutron/X-ray reflectivity data using MOTOFIT. *J. Appl. Crystallogr.* **2006**, *39*, 273–276.
40. Heavens, O.S. Optical properties of thin films. *Rep. Prog. Phys.* **1960**, *23*, 1–65.
41. Olivier, A.; Meyer, F.; Raquez, J.M.; Damman, P.; Dubois, P. Surface-initiated controlled polymerization as a convenient method for designing functional polymer brushes: From self-assembled monolayers to patterned surfaces. *Prog. Polym. Sci.* **2012**, *37*, 157–181.
42. Patten, T.E.; Xia, J.; Abernathy, T.; Matyjaszewski, K. Polymers with very low polydispersities from atom transfer radical polymerization. *Science* **1996**, *272*, 866–868.
43. Robinson, K.L.; Khan, M.A.; de Paz Banez, M.V.; Wang, X.S.; Armes, S.P. Controlled polymerization of 2-hydroxyethyl methacrylate by ATRP at ambient temperature. *Macromolecules* **2001**, *34*, 3155–3158.
44. Xia, J.; Gaynor, S.G.; Matyjaszewski, K. Acrylates at ambient temperature. *Macromolecules* **1998**, *31*, 5958–5959.
45. Jones, B.D.M.; Huck, W.T.S. Controlled surface-initiated polymerizations. *Adv. Mater.* **2001**, *13*, 1256–1259.
46. Huang, W.; Kim, J.B.; Bruening, M.L.; Baker, G.L. Functionalization of surfaces by water-accelerated atom-transfer radical polymerization of hydroxyethyl methacrylate and subsequent derivatization. *Macromolecules* **2002**, *35*, 1175–1179.
47. Xia, J.; Matyjaszewski, K. Controlled /living radical polymerization. Atom transfer radical polymerization using multidentate amine ligands. *Macromolecules* **1997**, *30*, 7697–7700.
48. Tang, W.; Matyjaszewski, K. Effect of ligand structure on activation rate constants in ATRP. *Macromolecules* **2006**, *39*, 4953–4959.
49. Paik, H.J.; Horwitz, C.P. Tridentate nitrogen-based ligands in Cu-based ATRP: A structure—Activity study. *Macromolecules* **2001**, *34*, 430–440.
50. Tang, W.; Matyjaszewski, K. Effects of initiator structure on activation rate constants in ATRP. *Macromolecules* **2007**, *40*, 1858–1863.
51. Xia, J.; Matyjaszewski, K. Controlled/"living" radical polymerization. Homogeneous reverse atom transfer radical polymerization using AIBN as the initiator. *Macromolecules* **1997**, *30*, 7692–7696.
52. Tang, W.; Nanda, A.K.; Matyjaszewski, K. Effect of [pyridylmethanimine]/[CuI] ratio, ligand, solvent and temperature on the activation rate constants in atom transfer radical polymerization. *Macromol. Chem. Phys.* **2005**, *206*, 1171–1177.

53. Kim, J.B.; Huang, W.; Miller, M.D.; Baker, G.L.; Bruening, M.L. Kinetics of surface-initiated atom transfer radical polymerization. *J. Polym. Sci. A* **2003**, *41*, 386–394.
54. Matyjaszewski, K.; Nanda, A.K.; Tang, W. Effect of [CuII] on the rate of activation in ATRP. *Macromolecules* **2005**, *38*, 2015–2018.
55. Nanda, A.K.; Matyjaszewski, K. Effect of [PMDETA]/[Cu(I)] ratio, monomer, solvent, counterion, ligand, and alkyl bromide on the activation rate constants in atom transfer radical polymerization. *Macromolecules* **2003**, *36*, 1487–1493.
56. Matyjaszewski, K.; Shipp, D.A.; Wang, J.L.; Grimaud, T.; Patten, T.E. Utilizing halide exchange to improve control of atom transfer radical polymerization. *Macromolecules* **1998**, *31*, 6836–6840.
57. Laurent, P.; Souharce, G.; Duchet-Rumeau, J.; Portinha, D.; Charlot, A. 'Pancake' *vs.* brush-like regime of quaternizable polymer grafts: An efficient tool for nano-templating polyelectrolyte self-assembly. *Soft Matter* **2012**, *8*, 715–725.
58. Bain, E.D.; Dawes, K.; Özçam, A.E.; Hu, X.; Gorman, C.B.; Šrogl, J.; Genzer, J. Surface-initiated polymerization by means of novel, stable, non-ester-based radical initiator. *Macromolecules* **2012**, *45*, 3802–3815.
59. Cheng, N.; Azzaroni, O.; Moya, S.; Huck, W.T.S. The effect of [CuI]/[CuII] ratio on the kinetics and conformation of polyelectrolyte brushes by atom transfer radical polymerization. *Macromol. Rapid Commun.* **2006**, *27*, 1632–1636.
60. Karg, M.; Schelero, N.; Oppel, C.; Gradzielski, M.; Hellweg, T.; von Klitzing, R. Versatile phase transfer of gold nanoparticles from aqueous media to different organic media. *Chemistry* **2011**, *17*, 4648–4654.
61. Enustun, B.V.; Turkevich, J. Coagulation of colloidal gold. *J. Am. Chem. Soc.* **1963**, *85*, 3317–3328.
62. Matyjaszewski, K.; Miller, P.J.; Shukla, N.; Immaraporn, B.; Gelman, A.; Luokala, B.B.; Siclovan, T.M.; Kickelbick, G.; Vallant, T.; Hoffmann, H.; *et al*. Polymers at interfaces: Using atom transfer radical polymerization in the controlled growth of homopolymers and block copolymers from silicon surfaces in the absence of untethered sacrificial initiator. *Macromolecules* **1999**, *32*, 8716–8724.
63. Rauch, S.; Uhlmann, P.; Eichhorn, K.J. *In situ* spectroscopic ellipsometry of pH-responsive polymer brushes on gold substrates. *Anal. Bioanal. Chem.* **2013**, *405*, 9061–9069.